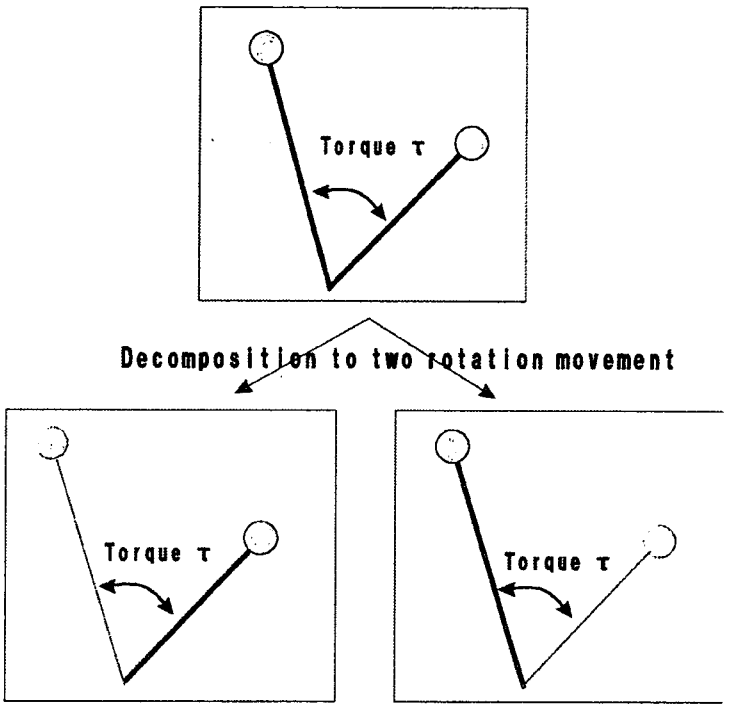

Figure 7. Relative rotational movement and internal force (torque).

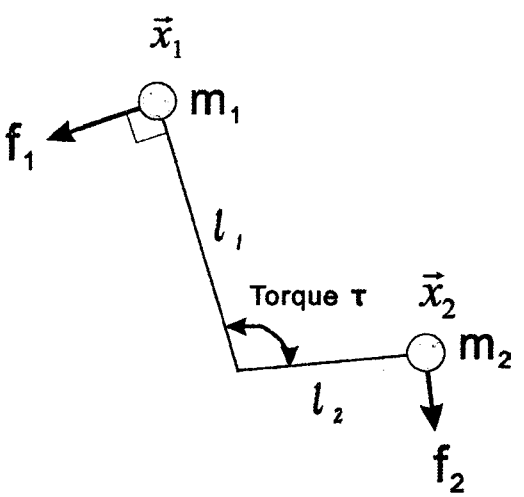

Figure 8. Influence on the two particles by the torque effect.

In general:

$$\vec{f}_1 = \frac{\tau}{l_1^2}\vec{n} \times \vec{x}_1 \tag{20}$$

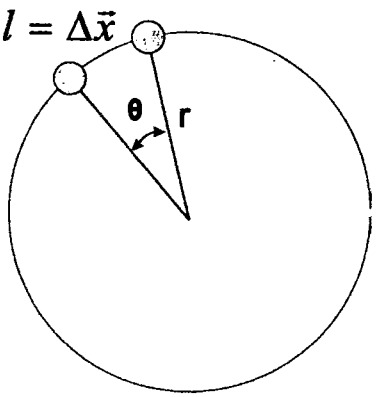

Figure 9. Rotation angle and angular velocity.

where $\vec{n}$ is the normal vector of the rotation plane, $\vec{x}_1$ is the position of the particle from the rotation center and l is the distance $l = |\vec{x}_1|$.

Two particles are effected by $\vec{f}_1$ and $\vec{f}_2$ calculated from Fig. 8:

$$\vec{f}_1 = \frac{\tau}{l_1^2}\vec{n} \times \vec{x}_1, \quad \vec{f}_2 = \frac{\tau}{l_2^2}\vec{n} \times \vec{x}_2 \tag{21}$$

By using this decomposition process, we can convert the torque effect to the force toward the two particles and we can describe the torque effect of the joint.

3.2. *Friction effect*

The next process is to describe the friction effect of the joint in the rotation movement. First, the friction effect is represented as:

$$\tau = -D\dot{\theta} \tag{22}$$

where D is the friction coefficient, θ is the rotation angle and τ is the torque. It is clear that $l = r \cdot \theta$ (Fig. 9):

$$\Delta l = r \cdot \dot{\theta} = \Delta\vec{x} \sim \dot{\vec{x}} \tag{23}$$

in the case of a very small time step.

In addition, by including the fact that one joint is constructed from three particle coordinates, the particle position $\vec{x}_1$, $\vec{x}_2$'s angular velocity $\vec{\theta}_1$, $\vec{\theta}_2$ seen from the rotation center $\vec{x}_2$ is directly connected with the joint angle velocity $\vec{\theta}$:

$$\dot{\theta}_1 = \frac{\Delta\vec{x}_1}{l_1} \sim \frac{\dot{\vec{x}}_1}{l_1}, \quad \dot{\theta}_2 = \frac{\Delta\vec{x}_2}{l_2} \sim \frac{\dot{\vec{x}}_2}{l_2} \tag{24}$$

The torque value calculated from the friction effect of the joint is:

$$\tau^{\text{friction}} = -\frac{D}{l_1}(\dot{\vec{x}}_1 - \dot{\vec{x}}_2) \tag{25}$$

$$-\frac{D}{l_2}(\dot{\vec{x}}_3 - \dot{\vec{x}}_2) \tag{26}$$

By adding this effect to (21), we can include the friction effect in the multi-link movement dynamics.

4. SINGLE-LINK MOVEMENT CONTACT WITH FLOOR

In this section, we simulate a single-link system movement which is constructed from three particles, and confirm it under the condition of a free-fall state to touch and bounce off the floor. Figure 10 shows the movement of the single-link system. In the first phase, the link system falls down due to gravity (phase 1). This effect is realized by adding the gravity effect to the motion equation:

$$m_i \frac{\mathrm{d}x^2}{\mathrm{d}t^2} = F_x \tag{27}$$

$$m_i \frac{\mathrm{d}y^2}{\mathrm{d}t^2} = F_y \tag{28}$$

$$m_i \frac{\mathrm{d}z^2}{\mathrm{d}t^2} = F_z + m_i g \tag{29}$$

where m_i is the mass of each of the particles, g is the gravity constant and (F_x, F_y, F_z) means the calculated force from (21) or spring–damper effect. The next phase is to touch the floor. The third particle contacts with and bounces off the floor. In this phase, we use the floor effect as:

$$\frac{\mathrm{d}z}{\mathrm{d}t} = \begin{cases} \dfrac{\mathrm{d}z}{\mathrm{d}t} & (z > \text{floor height}) \\ -0.8\dfrac{\mathrm{d}z}{\mathrm{d}t} & (z < \text{floor height}) \end{cases} \tag{30}$$

This is just an inelastic collision. In the third phase, the collision effect is transmited to other particles by the spring system and particle 2 shifts position to the right direction. In our proposed model, it is very easy to include these external effects as the force effect to each of the particles. For example, the effect of floor contact can be changed to an elastic collision, spring-type floor or non-linear deformation.

5. WALKING MOVEMENT OF THE HUMAN LINK MODEL

In this section, we construct an eight-particle link model which is shown in Fig. 11. This model has six rotation joints, p(1)–p(2)–p(3) represents a single joint, and each of the joints has friction and we can give a torque for each of the joints. The link length is 10 [p(1)–p(2) and p(8)–p(7):foot position], 50 [p(2)–p(3) and p(6)–p(7):leg], 40 [p(3)–p(4) and p(5)–p(6):hip], 20 [p(4)–p(5):hip joint width] in this

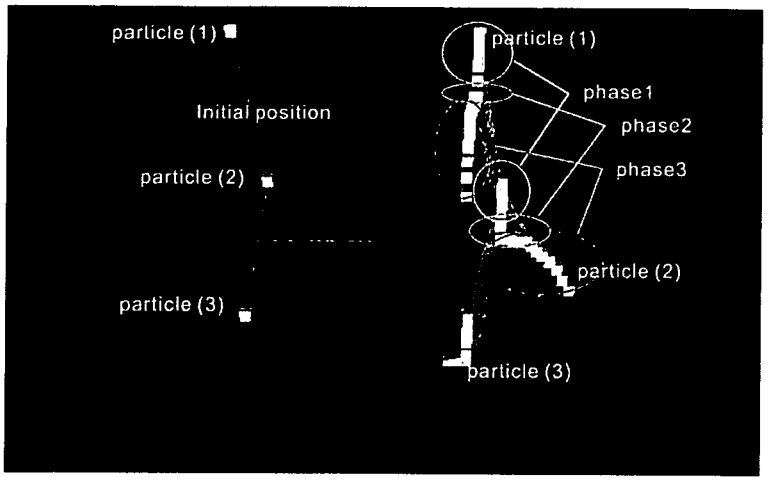

Figure 10. Single link movement contact with the floor under the effect of gravity.

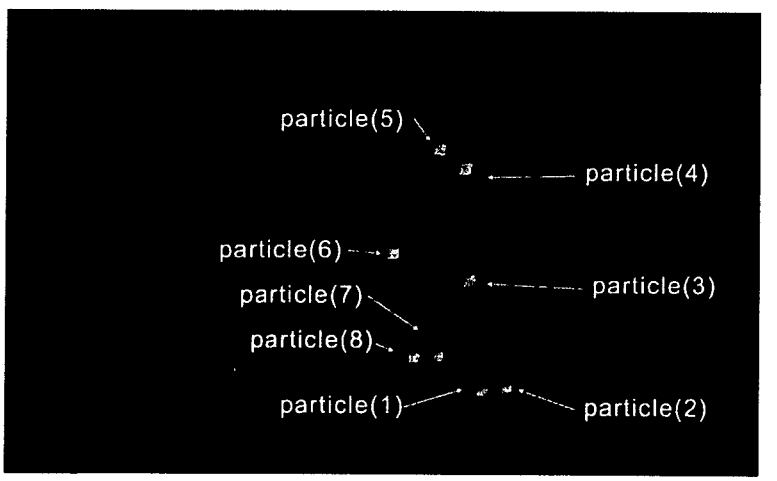

Figure 11. Human link model constructed of eight particles.

model (more detailed parameters are shown in Table 1). Figure 12 shows the free-fall phase of the simulation. The human model falls down and touches the floor. The floor is a simple spring system and each of the particles is effected by the criterion condition such as (30). We define the mass of the p(1)–p(3) and p(6)–p(8) as 1.0, and p(4)–p(5) as 10.0.

The next phase represents the walking movement in which the right leg is in the support phase and the left leg is in the swing phase (Fig. 13). In this simulation, the walking motion plan is given by an operator beforehand in order that the zero moment point [13] is under the foot's support polygon and each of the joint torques is determined by a simple PD feedback rule to realize the planned motion.

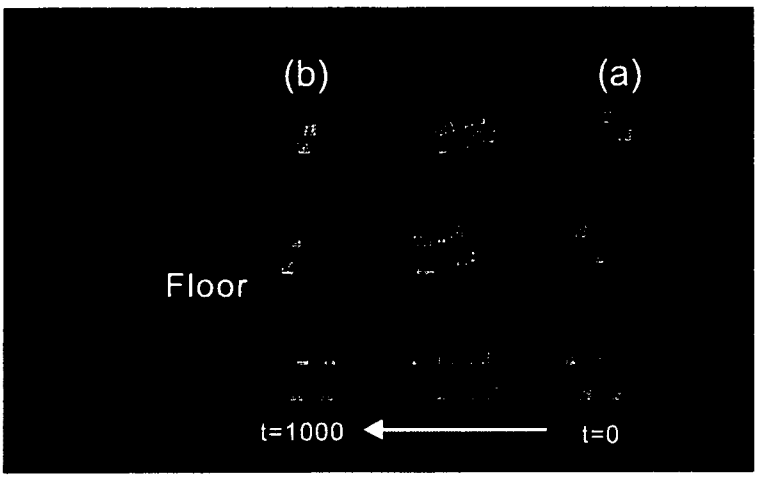

Figure 12. Free-fall phase. (a) Initial state ($t = 0$). (b) The model touches the floor and holds the standing state ($t = 1000$).

Table 1.
Precise model parameters

Parameter	Link connection	Value
Length	p(1)–p(2), p(7)–p(8)	10
Length	p(2)–p(3), p(6)–p(7)	50
Length	p(3)–p(4), p(5)–p(6)	40
Length	p(4)–p(5)	20
Mass	p(1)–p(3), p(6)–p(8)	1
Mass	p(4)–p(5)	10
Joint friction	p(1)–p(2)–p(3), p(2)–p(3)–p(4)	5.0
Joint friction	p(3)–p(4)–p(5), p(4)–p(5)–p(6)	5.0
Joint friction	p(5)–p(6)–p(7), p(6)–p(7)–p(8)	5.0

In order to realize forward walking movement of the human model, a friction effect formed by a foot contact with the floor is needed. If a particle is contacting with the floor (the walk direction is x) and the vertical component of the ground reaction force is T_z:

$$f_x = -\gamma \cdot \frac{\mathrm{d}x}{\mathrm{d}t} \cdot T_z \tag{31}$$

where f_x is the reaction force of the particle from the floor, γ is the friction drag and $\frac{\mathrm{d}x}{\mathrm{d}t}$ is the velocity. The ground reaction force is represented by:

$$T_z = \begin{cases} m_i \vec{a}_i \cdot \vec{n}_z & z \leqslant \text{floor height} \\ 0 & z > \text{floor height} \end{cases} \tag{32}$$

where $\vec{n}_z$ is the normal vector of the floor and $\vec{a}_i$ is the particle's acceleration.

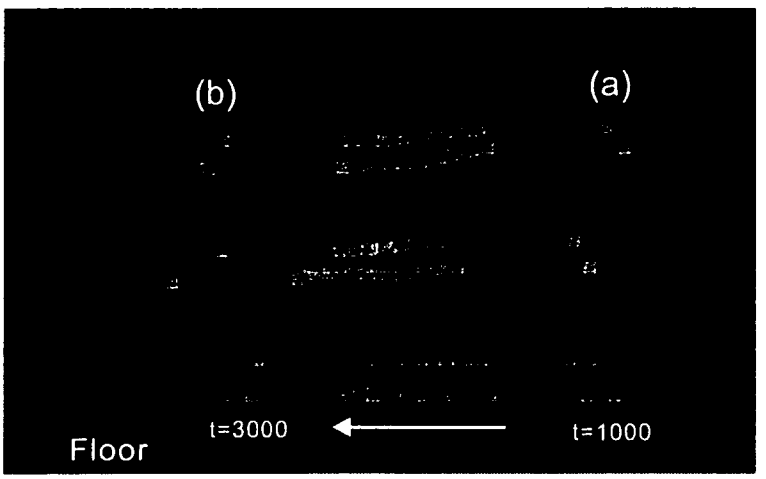

Figure 13. Walking movement phase 1. (a) Initial state ($t = 1000$). (b) Final state ($t = 3000$).

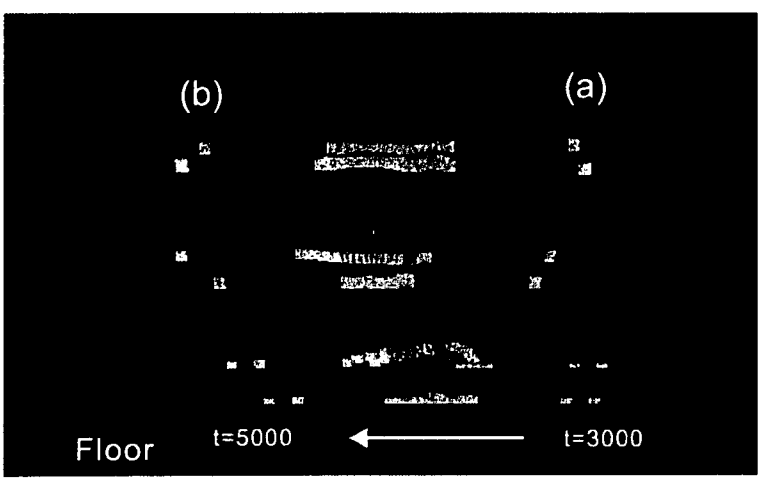

Figure 14. Walking movement phase 2. (a) Initial state ($t = 3000$). (b) Final state ($t = 5000$).

Figure 14 shows the walking movement when the right leg is in the swing phase and the left leg is in the support phase. The torque response curve of the support and the swing leg is shown in Fig. 15 from the free-fall phase ($t = 0 \rightarrow t = 1000$) to the first walking motion phase ($t = 1000 \rightarrow t = 3000$).

6. DISCUSSION

In our proposed model, the effect of the moment of inertia has not yet been defined. However, since the moment of inertia can be understand as the difficulty of rotating an object, it is possible to convert it as the torque effect (Section 3.1) such as the friction (Section 3.2). For example, we can convert the inertia as a single large mass

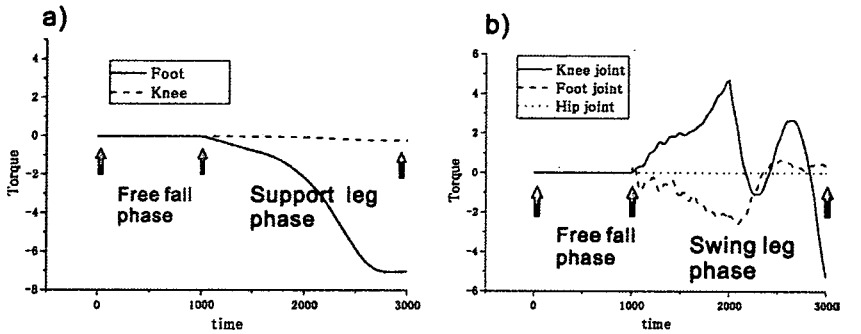

Figure 15. Torque response of the support leg (a) and the swing leg (b) in walking movement (from $t = 0$ to $t = 3000$).

in the case when the center of the rotation is defined. If the mass is positoned at the terminus of the link, we can calculate the conversion mass m:

$$I = m \cdot l^2 \Leftrightarrow m = \frac{I}{l^2} \tag{33}$$

where l is the link length and I is the moment of inertia. By using this method, we can include the effect of the moment of inertia. With regard to the computational cost, the order of the forward kinematics calculations of multi-link system is about $O(n)$ and the order is changed to $O(n^2)$ in the case that there are restriction conditions [9, 10]. However, the order of the our proposed method is $O(n)$ under the restriction conditions and this is another advantage of our proposed method.

7. CONCLUSIONS

In this paper, we propose a new three-dimensional multi-link movement simulator. Our proposed method considers the multi-link system as a multi-particle movement system which each of the particles being connected by a simple spring–damper model. By including the rotation plane in this model, we can treat the revolute joint, and represent the effect of the torque and the friction. By using this assumption, it is not necessary to use the Jacobian matrix for calculating the link dynamics and it is very easy to manage many of external effects, such as the floor, external shock or gravity effect, as external forces toward each of the particles. These features play an important role in the complex dynamics simulation of the multi-link system, especially in the case of a large numner of links. Through experiments with the multi-link dynamics simulation, we confirmed the effectiveness of the proposed method. This means that the work space representation of the multi-link system is more useful for the movement dynamics simulation as compared with the angle state space representation.

REFERENCES

1. Y. Sugahara, T. Endo, H.-o. Lim and A. Takanishi, Design of a battery-powered multi-purpose bipedal locomotor with parallel mechanism, in *Proc. IEEE/RSJ Int. Conf. on Intelligent Robots and Systems*, pp. 2658–2663 (2002).
2. H. Inoue, HRP: humanoid robotics project of MITI, in *Proc. 1st IEEE–RAS Int. Conf. on Humanoid Robots* (2000).
3. Y. Sakagami, R. Watanabe, C. Aoyama, S. Matsunaga, N. Higaki and K. Fujita, The intelligent ASHIMO: system overview and integration, in *Proc. IEEE/RSJ Int. Conf. on Intelligent Robots and Systems*, pp. 2478–2483 (2002).
4. J.-H. Kim and J.-H. Oh, Torque feedback control of the humanoid platform KHR-1, in *Proc. 3rd IEEE Int. Conf. on Humanoid Robots*, pp. 00–00, Karlsruhe and Munich (2003).
5. T. Inamura, I. Toshima and Y. Nakamura, Acquisition and embodiment of motion elements in closed mimesis loop, in *Proc. IEEE Int. Conf. on Robotics and Automation*, pp. 1539–1544 (2002).
6. F. Kanehiro, K. Fujiwara, S. Kajita, K. Yokoi, K. Kaneko and H. Hirukawa, Open architecture humanoid robot platform, in *Proc. Int. Conf. on Robotics and Automation* (2002).
7. S. Kajita, O. Matsumoto and M. Saigo, Real-time 3D walking pattern generation for a biped robot with telescopic legs, in *Proc. IEEE Int. Conf. on Robotics and Automation*, pp. 2299–2036 (2001).
8. K. Yamane and Y. Nakamura, Dynamic filter — concept and implementation of on-line motion generator for human figures, in *Proc. IEEE Int. Conf. on Robotics and Automation*, pp. 688–695, San Francisco, CA (2000).
9. R. Featherstone, *Robot Dynamics Algorithms*, Kluwer, Dordrecht (1987).
10. M. W. Walker and D. E. Orin, Efficient dynamic computer simulation of robotic mechanisms, *J. Dyn. Syst. Meas. Control* **104**, 205–211 (1982).
11. K. Yamane and Y. Nakamura, Dynamics filter oncept and implementation of on-line motion generator for human figures, in *Proc. IEEE Int. Conf. on Robotics and Automation*, pp. 688–694 (2000).
12. Y. Fujimoto and A. Kawamura, Simulation of an autonomous biped walking robot including environmental force interaction, *IEEE Robotics Automat. Mag.* (June), 33–42 (1998).
13. M. Vukobratovic and J. Stepanenko, On the stability of anthropomorphic systems, *Math. Biosci.* **15**, 1–37 (1972).

ABOUT THE AUTHORS

Hideki Toda belongs to the Doctoral Program of Systems and Information Engineering of Sankai Laboratory University of Tsukuba, Tsukuba, Japan.

Yoshiyuki Sankai received the PhD degree in Engineering from the University of Tsukuba, Japan in 1987. He was named a JSPS fellow, Research Associate and Associate Professor in University of Tsukuba. He is a Visiting Professor at Baylor College of Medicine, USA and Ordinary Professor at the Institute of Systems and Engineering Mechanics, University of Tsukuba, Japan. His research interests include assistive exoskeletal robots, the next generations of artificial hearts and humanoids as related fields of cybernetics. He received the JSAO Grant of the Japanese Society for Artificial Organs, and Awards from the American Society for Artificial Organs, International Society for Artificial Organs and International Society for Rotary Blood Pump with his students. He is a Chair of Japan Society of Embolus Detection and Treatment, Vice Chair of the International Journal of the Robotics Society of Japan, Member of the Awards Committee of the Japan Society of Mechanical Engineers, and Member of the Assessment Committee of the New Energy and Industrial Technology Development Organization, Japan.

Advanced Robotics, Vol. 20, No. 6, pp. 661–679 (2006)

Also available online - www.vsppub.com

Full paper

A multi-link system control strategy based on biological reaching movement

HIDEKI TODA [1], TATSU KOBAYAKAWA [2] and YOSHIYUKI SANKAI [1,*]

[1] *Doctoral Program of Systems and Information Engineering, Sankai Laboratory, University of Tsukuba, Tsukuba, Ibaraki 305-0006, Japan*
[2] *Multimodal Integration Research Group, Institute for Human Science and Biomedical Engineering, National Institute of Advanced Industrial Science and Technology, AIST Tsukuba Central 6, Tsukuba, Ibaraki 305-8561, Japan*

Received 12 May 2005; accepted 22 July 2005

Abstract—In the multi-link arm control process, the problems of trajectory planning and trajectory realization have been recognized as being of key importance. We developed a technique by which to realize a reaching movement control of the multi-link arm system, which was inspired by experimental results for reaching movements of macaques or human beings. The proposed method can treat the effect of the dynamics of the multi-link system and the trajectory planning of the end-effector, which has a bell-shaped speed profile, as well as the difficulties of redundancies of multi-link systems. Two-link arm reaching movement experiments revealed the same features, as demonstrated by the results of biological experiments on humans and macaques. In addition, the results obtained using a two-dimensional four-link model in a standing-up movement control experiment agreed well with 'standing-up from a chair' movement of human beings. Since the proposed method has a simple structure and its implementation process is simple, the proposed method will be effective for use in a multi-link system control strategy.

Keywords: Multi-link control; biologically inspired control; bell-shaped speed profile.

1. INTRODUCTION

Many creatures, including human beings, realize movement through multi-link systems, or what are usually referred to as 'arms' or 'legs'. Interpreting the control planning and executive system of a creature as a control system is useful for understanding the control strategy of the cerebellum as well as for application to machine systems used by humans, e.g., walking assist systems [1] or artificial limbs (Fig. 1).

*To whom correspondence should be addressed. E-mail: sankai@golem.kz.tsukuba.ac.jp

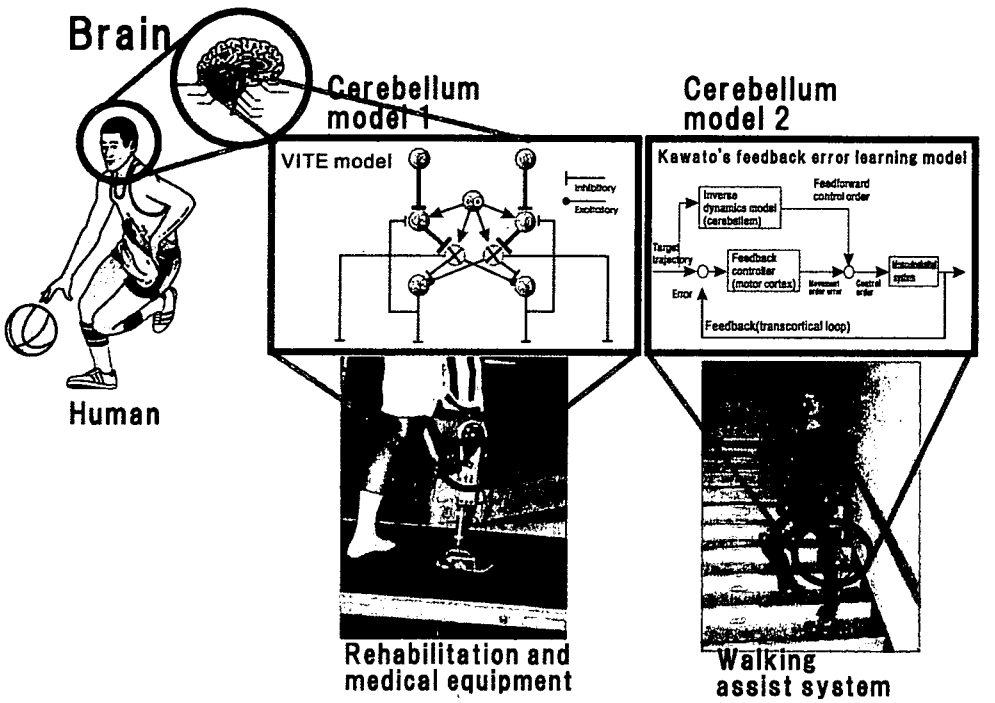

Figure 1. Mathematical approach based on biological models.

Manipulator control has been investigated for decades [2]. Volpe and Khosa [3] show that general impedances are useful for manipulator control, and a neural oscillator model [4] has been used to exploit the intrinsic dynamics of the control process. Approaches involving the cerebellum model [5–7] have been used for motion creation and as a control model. Studies of the kinematic and dynamic aspects of the planar, unconstrained multi-link arm movements of humans and monkeys [8, 9] have shown some features such as:

- Straight-line hand trajectory.
- Single-peaked, bell-shaped speed profile of hand trajectory.

Bernstein [10] stated that there are three problems in multi-link system movement control. The first involves how the central nervous system (CNS) selects a specific hand trajectory from the infinite number possibilities in moving from one point to another. The second involves how the CNS determines the joint angle combinations in order to realize the hand trajectory. The third involves how the CNS realizes the desired trajectory by giving motor control commands to the muscles. Trajectory planning and the trajectory realization process are ill-posed problems and a unique solution to these problems cannot be found.

From a biological perspective, a number of biomechanics models for multi-link system control have been proposed, including the VITE/FLETE model by Bullock and Grossberg [11], the equilibrium point hypothesis/control theory [12–14] and

the minimum torque change criterion model, proposed by Kawato *et al.* [15] and Uno *et al.* [16]. Biological experiments examining monkey elbow movements have indicated that the CNS generates control signals that define a series of equilibrium positions [17] and Feldman [18] realized two-link arm reaching movement control by using the equilibrium point hypothesis/control theory. According to the equilibrium point hypothesis, Hogan [19] used the 'minimum jerk criterion' rule to determine an ideal trajectory plan from the initial position to the final position of the arm which had a 'bell-shaped' speed profile property. Generally, movement control is constructed from two execution processes, which are divided into each other functionally. The first process is trajectory planning, which corresponds to the VITE model and the minimum jerk criterion rule. The second process is the movement realization process, the FLETE model and a kind of torque criterion or torque smoothness cost function that is used in conjunction with the model. The trajectory planning process is treated using static trajectory planning algorithms, which depend on work space coordinates and are independent of the dynamics of the multi-link system. In addition, these two problems are not clearly separable. Therefore, rather than handling the two processes using different algorithms, we propose a controller that has a trajectory generating function. In this controller, the force decision process is executed while performing the trajectory planning process.

2. THEORY

A diagram of the proposed multi-link system controller is shown in Fig. 2. The system controller is constructed from a trajectory planning controller and a trajectory realization controller. These two controllers receive the position, velocity and acceleration information of the end-effector of a multi-link system. The trajectory planning controller uses this information to decide the ideal trajectory of the end-effector as the force $\vec{f}$ of the end-effector and the trajectory realization controller uses this information to determine all of the joint torques $\vec{\tau}$ of the multi-link system. The proposed controller realizes multi-link reaching movement using

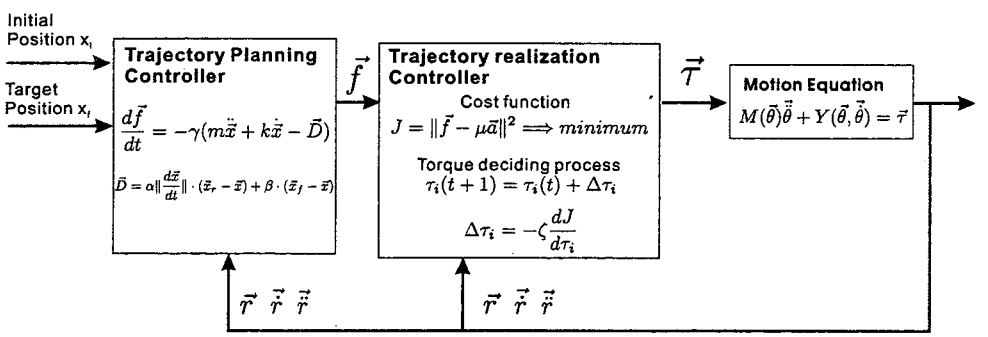

Figure 2. Block diagram of the proposed trajectory planning and realization.

only the acceleration of the end-effector. This mechanism can reduce the controller design complexity compared to previously proposed techniques, such as that of Ma [20]. However, instabilities due to simplicity must be avoided. The proposed controller manages instability by using a controller having the function of trajectory generation. In addition, the trajectory realization controller also determines the joint torques using only the acceleration of the end-effector and instabilities such as inverse kinematics are managed by the trajectory planning controller. In many cases, a previously proposed multi-link system controller is used to calculate the static ideal trajectory plan before the movement and multi-link movement is realized by following the calculated ideal trajectory plan (e.g., Fagg *et al.* [5]). This mechanism, however, has disadvantages for external disturbances and a calculation error of the inverse kinematics of the multi-link dynamics. The strategy of the proposed method does not realize the multi-link movement by resolving the inverse kinematics of the system and then controlling all of joints angles to previously calculated joint angles. Rather, the proposed method conveys only the end-effector position of the multi-link system from the initial position to the target position by using the acceleration information of the end-effector.

2.1. Trajectory planning controller

The proposed controller determines the present control order by using the information of the present hand position and the speed vector of the end-effector in the work space. We defined the control rule as follows:

$$\vec{f}^{\,\text{bell}} = \alpha \left\| \frac{\mathrm{d}\vec{x}}{\mathrm{d}t} \right\| \cdot (\vec{x}_\mathrm{r} - \vec{x}) + \beta \cdot (\vec{x}_\mathrm{f} - \vec{x}), \tag{1}$$

where α and β are positive small constants, $\vec{f}$ is the force vector of the end-effector of the hand, and $\vec{x}$, $\vec{x}_\mathrm{i}$ and $\vec{x}_\mathrm{f}$ are the present initial and final positions of the end-effector of the hand, respectively. We herein set $\vec{x}_\mathrm{r} = (\vec{x}_\mathrm{i} + \vec{x}_\mathrm{f})/2$ as the reference position. Through an experiment examining reaching movement control in one-dimensional (1D) space, we confirm the validity of (1) by comparison with the PD control method.

The motion equation of a particle in 1D space is $m(\mathrm{d}^2x/\mathrm{d}t^2) = -k(\mathrm{d}x/\mathrm{d}t) + f_x$, where x, m and k are the position, mass and coefficient of friction of the system, respectively. In this case, we define $f_x = \alpha\|\mathrm{d}x/\mathrm{d}t\| \cdot (x_\mathrm{r} - x) + \beta \cdot (x_\mathrm{f} - x)$ from equation (1). The position, velocity and force of the proposed controller are shown in Fig. 3 for the case in which $m = 5$, initial position $x_\mathrm{i} = 0$, final position $x_\mathrm{f} = 10$, time step $\Delta t = 0.001$, $\alpha = 1.0$, $\beta = 0.001$ and $k = 0$.

The primary differences from the simple PD controller are the velocity and force profiles. The velocity distribution of the proposed controller has a symmetric bell-shape and the force has a reverse distribution at the reference point (x_r). These features are not seen in the simple PD controller.

For further clarification, we compared the proposed controller (Fig. 4) with the LQR controller (Fig. 5) under the condition of the 1D reaching movement

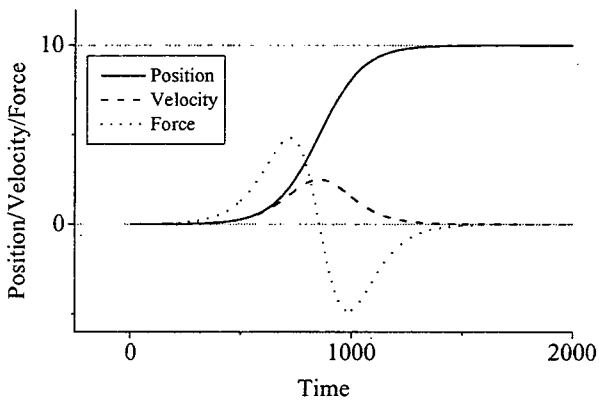

Figure 3. One-dimensional reaching movement of the proposed controller.

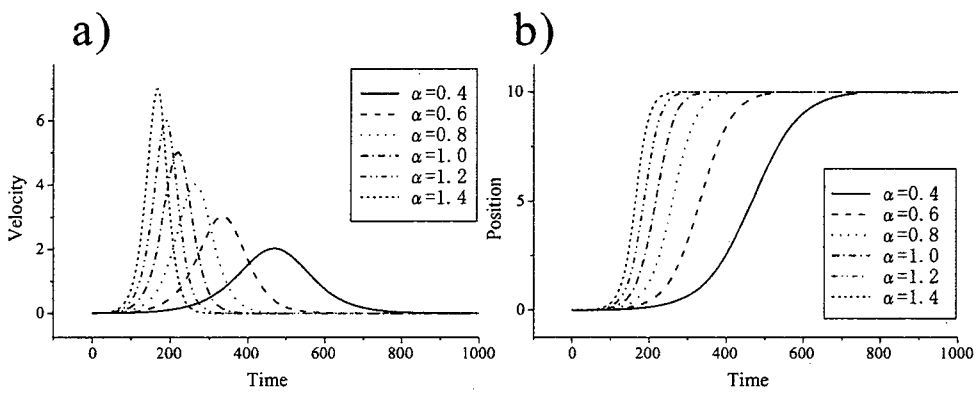

Figure 4. Parameter dependency of our proposed speed profile control method on (a) velocity and (b) position.

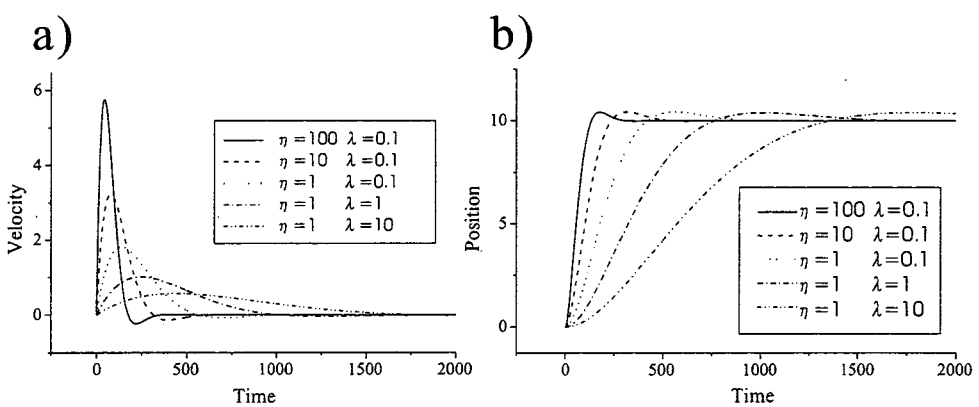

Figure 5. Parameter dependency of the LQR method on (a) velocity and (b) position transition.

($m = 20, k = 0, \Delta t = 0.001, x_i = 0, x_f = 10$). Here, we set a cost function as $J = \int_0^{t_f} \vec{x}^T Q \vec{x} + \vec{u}^T R \vec{u}\, dt$, where

$$Q = \begin{bmatrix} \eta & 0 \\ 0 & 1/\eta \end{bmatrix}$$

and $R = \lambda$. In this experiment, the LQR controller is defined as $f_x^{PD} = K_p(x_f - x) + K_d \dot{x}$, and we set the feedback gain K_p and K_d for minimizing the cost function Q in the case of constant parameter η, λ:

$$\begin{bmatrix} \eta \\ \lambda \end{bmatrix} = \begin{bmatrix} 100 \\ 0.1 \end{bmatrix}, \begin{bmatrix} 10 \\ 0.1 \end{bmatrix}, \begin{bmatrix} 1 \\ 0.1 \end{bmatrix}, \begin{bmatrix} 1 \\ 1 \end{bmatrix}, \begin{bmatrix} 1 \\ 10 \end{bmatrix}.$$

The dependency of the parameter $\alpha = 0.4, 0.6, 0.8, 1.0, 1.2$ and 1.4 of the proposed method is shown in Fig. 4 for comparing with the LQR controller. The parameter β always takes the value of $1/100$ or less and we set $\beta = 0.01$ in this experiment. In principle, the parameter β is used in order to obtain a small initial velocity and to hold the particle at the final position.

In order to understand the difference of the two control strategies, we compared the strategies with respect to force transition. The force transitions of a reaching movement under the condition of the same settling time are shown in Fig. 6. The settling time is decided by the condition that a local standard deviation

$$\sigma(t) = \sqrt{\frac{\sum_t^{t+\Delta s} (x(t) - \vec{x}_f)^2}{\Delta s^2}} \text{ takes } < 0.01$$

and the time step Δs is 100. The settling time is $t_f = 2003$ in the case of the LQR controller $\eta = 1, \lambda = 1$, and $t_f = 1995$ in the case of the proposed method $\alpha = 0.8$. By comparing the torque cost function $J = (1/2)\int_0^{t_f} \vec{\tau}^T \vec{\tau}\, dt = (1/2)\int_0^{t_f} f_x^2\, dt$, which was used as a performance function of the multi-link movement strategy, the LQR controller shows $J_{PD} = 10.538$ and the proposed controller shows $J_{bell} = 5.975$. This means that an improvement of approximately 45% is found and this improvement has a tendency to disappear when the settling time becomes long. The strategic difference from the LQR control in the initial movement is

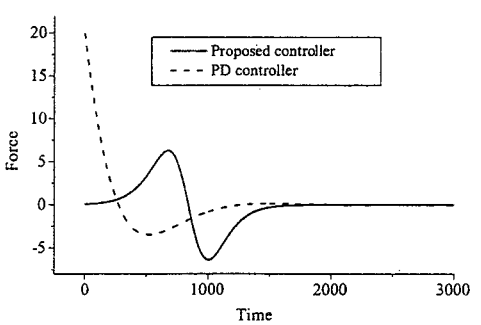

Figure 6. Comparison of the force transition between the proposed controller and the LQR controller.

emphasized in the case of a short settling time condition. This mechanism is useful for constructing a low-damage movement control system, and a reasonable and unstrained movement for a biological system.

The proposed controller, however, cannot manage with external disturbances such as gravity effects, and we introduce a compensator against external disturbances. If the motion equation of the particle is represented as $m\ddot{x}(t) + k\dot{x}(t) + d(t) = f(t)$, the force $f(t)$ is adjusted by:

$$\frac{df}{dt} = -\gamma\left[m\ddot{x} + k\dot{x} - D(t)\right],$$
$$D(t) = \alpha\left\|\frac{dx}{dt}\right\| \cdot (x_r - x) + \beta \cdot (x_f - x), \tag{2}$$

where γ is a positive constant and $D(t)$ is the proposed control term. This works as a simple external disturbance compensator. Since this mechanism needs the present particle acceleration $\ddot{x}(t)$ and velocity $\dot{x}(t)$, we must know the information by observing sensors.

2.2. *Trajectory realization controller*

The motion equation of a two-link system (Fig. 7) is represented as:

$$M(\vec{q})\ddot{\vec{q}} + C\left(\dot{\vec{q}}, \vec{q}\right)\dot{\vec{q}} = \vec{\tau}, \tag{3}$$

where $\vec{q} = (\theta_1, \theta_2)$ represents the joint angle, $M \in R^{2\times 2}$ is an inertia matrix, $C(\dot{\vec{q}}, \vec{q}) \in R^{2\times 2}$ is a centrifugal, Coriolis and friction force, and $\vec{\tau} = (\tau_1, \tau_2)$ is a joint torque generated by agonist and antagonist muscles.

First, the process of the proposed controller is to derive a direct relation within the angular acceleration vector $\ddot{\vec{q}}$ and the torque $\vec{\tau}$, which is extracted from the motion equation (3):

$$\vec{\tau} = M(\vec{q})\ddot{\vec{q}}. \tag{4}$$

This simplification does not consider the effect of Coriolis, friction or centrifugal forces. If we can measure the precise joint friction or the centrifugal effect acting on a robot or a creature, then the inverse dynamics will be important for the torque decision process. The inverse dynamics problem is, however, difficult practically and does not work effectively in most real-world reaching movement process. Conversely, this simplification does not consider those dynamics positively, but rather is compensated for by the trajectory planning controller through the acceleration information of the end-effector.

Second, the end-effector position in 2D space (Fig. 7) is represented as:

$$\vec{x} = \begin{pmatrix} l_1\cos\theta_1 + l_2\cos(\theta_1 + \theta_2) \\ l_1\sin\theta_1 + l_2\sin(\theta_1 + \theta_2) \end{pmatrix}. \tag{5}$$

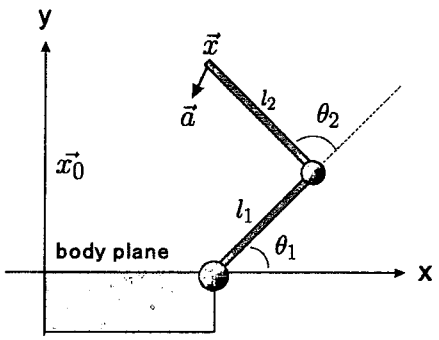

Figure 7. Two-link arm model in 2D space.

The acceleration of the end-effector can be calculated from (5) by taking the time derivative:

$$\vec{a} = \begin{pmatrix} a_x \\ a_y \end{pmatrix} = \begin{pmatrix} -l_1 \cos\theta_1 \dot{\theta_1}^2 - l_1 \sin\theta_1 \ddot{\theta_1} \\ -l_2 \cos(\theta_1 + \theta_2)(\dot{\theta_1} + \dot{\theta_2})^2 \\ -l_2 \sin(\theta_1 + \theta_2)(\ddot{\theta_1} + \ddot{\theta_2}) \\ -l_1 \sin\theta_1 \dot{\theta_1}^2 + l_1 \cos\theta_1 \ddot{\theta_1} \\ -l_2 \sin(\theta_1 + \theta_2)(\dot{\theta_1} + \dot{\theta_2})^2 \\ +l_2 \cos(\theta_1 + \theta_2)(\ddot{\theta_1} + \ddot{\theta_2}) \end{pmatrix}, \tag{6}$$

where l_1 and l_2 are the length from the shoulder to the elbow and from the elbow to the hand, respectively, and θ_1 and θ_2 are the angles of the shoulder and the elbow, respectively.

The third process is to define the cost function of the proposed method:

$$J = \|\vec{f} - \mu\vec{a}\|^2 = (f_x - \mu a_x)^2 + (f_y - \mu a_y)^2, \tag{7}$$

where $\vec{f}$ indicates the multi-dimensional form of the proposed trajectory planning algorithm (2), which is rewritten as:

$$\begin{aligned} \frac{\mathrm{d}\vec{f}}{\mathrm{d}t} &= -\gamma\left[m\dddot{\vec{x}} + k\dot{\vec{x}} - \vec{D}(t)\right], \\ \vec{D}(t) &= \alpha\left\|\frac{\mathrm{d}\vec{x}}{\mathrm{d}t}\right\| \cdot (\vec{x}_\mathrm{r} - \vec{x}) + \beta \cdot (\vec{x}_\mathrm{f} - \vec{x}), \end{aligned} \tag{8}$$

where $\vec{a}$ is the end-effector acceleration of (6) and μ is a positive constant.

In the control strategy, each joint torque is decided in order to minimize the cost function J and the least descent method is used for this purpose:

$$\begin{aligned} \vec{\tau}(t + \Delta t) &= \vec{\tau}(t) + \Delta\vec{\tau} \\ \Delta\vec{\tau} &= -\zeta\frac{\mathrm{d}J}{\mathrm{d}\vec{\tau}}, \end{aligned} \tag{9}$$

where ζ is a positive constant and Δt is a small time step. According to (9), the cost function value can be reduced in a step-by-step manner. The term $\mathrm{d}J/\mathrm{d}\vec{\tau}$ is

calculated from:

$$\frac{\mathrm{d}J}{\mathrm{d}\vec{\tau}} = \frac{\mathrm{d}J}{\mathrm{d}\vec{a}} \cdot \frac{\mathrm{d}\vec{a}}{\mathrm{d}\vec{\tau}} = \frac{\mathrm{d}J}{\mathrm{d}\vec{a}} \cdot \frac{\mathrm{d}\vec{a}}{\mathrm{d}\ddot{\vec{\theta}}} \cdot \frac{\mathrm{d}\ddot{\vec{\theta}}}{\mathrm{d}\vec{\tau}}, \tag{10}$$

using (4), (6) and (7).

Previously proposed models, such as equilibrium control [14], control all joint angles so as to follow an ideal trajectory plan for all joint angles in angular space coordinate. In contrast, the proposed method uses only the ideal trajectory of the end-effector of the multi-link system in work space coordinates. Experimental results [8, 17] for a biological system using a 'work space coordinate', rather than an 'angular space coordinate', have shown a certain validity. These experiments demonstrate that a visual coordinate, i.e., the arm position from the viewing eye, is used for control in biological systems. The advantage of not using angular space coordinates is avoiding the accumulation error by increasing the number of links, avoiding the singularity of the inverse dynamics and eliminating the need to precisely decide the friction or the viscosity by observation of the system. In contrast, the advantage of using the work space coordinates is that considering the spatial position of the arm is easier than considering the angular space coordinates. Treating the end-effector position as the center of the control point avoids the need to manage the entire link system dynamics and simplifies the control problem, reducing the computational cost.

3. TWO-LINK ARM MOVEMENT

The reaching movement control experiment for a two-link system in 2D space, which is the simplest redundant system, is shown in Fig. 8. Here, $l_1 = 40, l_2 = 40, m_1 = 10, m_2 = 10$, the joint frictions are $k_1 = 600$ and $k_2 = 600$, and the time step is $\Delta t = 0.001$. The control parameters are $\alpha = 0.7$, $\beta = 0.01$, $\mu = 1.0$ and $\gamma = 10$. In addition, the bell-shaped speed profile control parameters are $\alpha = 1.0$ and $\beta = 0.01$, and the cost function parameter μ is 1.0. Figure 8a shows the results of the reaching movement control experiment for the case in which the initial position $\vec{x}_\mathrm{i} = (4.7, 13.1)$ is the position of the right hand in front of the body and the target position $\vec{x}_\mathrm{f} = (41.5, 68.3)$ is the position of the right hand stretched to the front-right of the initial position. The results of this experiment show that the trajectory path of the bell-shaped speed profile distribution of the end-effector is extended slightly upward.

Figure 8b shows the case in which the initial position is $\vec{x}_\mathrm{i} = (0, 14)$ and the target position is $\vec{x}_\mathrm{f} = (0.036, 46.48)$. This movement is such that the arm is stretched forward from the initial position. The movement shows an almost perfect bell-shaped speed profile pattern and the trajectory of the end-effector is almost a straight line. Figure 8c shows the case in which the arm is stretched to the front-right from the initial position. The trajectory shows a slight swell compared to the

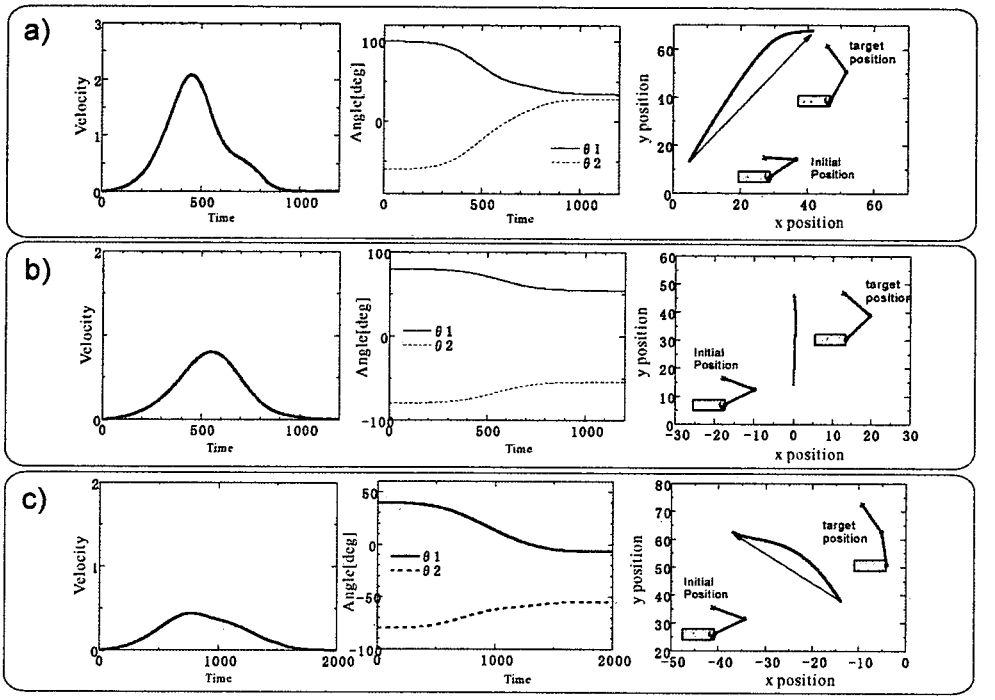

Figure 8. Two-link arm reaching movements in 2D space. Stretching direction: (a) front-right, (b) front and (c) front-left. The graphs give the speed profile of the end-effector, the angle transition and the position of the end-effector from the left.

movement to the front-right and the velocity profile is more similar to the bell-shape of the movement to the front. These trajectory shape features have been reported in Refs [8, 17, 21].

4. DEPENDENCY OF THE CONTROL SPEED

In the two-link reaching movement control under gravity the parameters are same as the two-link movement in a horizontal plane, except for $\alpha = 0.1$ (slow) and $\alpha = 0.3$ (fast) conditions, as shown in Fig. 9. Even under gravity, the proposed control strategy (7) and (9) requires no changes. However, the motion equation of the arm under gravity is of the form:

$$M(\vec{q})\ddot{\vec{q}} = C(\vec{q}, \dot{q}) + \vec{G} + \vec{\tau}, \tag{11}$$

where the term $\vec{G}$ is the gravity force element related to the shoulder and elbow angles θ_1 and θ_2, respectively. In this experiment, the initial position is equivalent to the arm being parallel to the line of the body and the target position is at approximately shoulder height, perpendicular to the line of the body. The trajectory of the end-effector is arc-shaped and is affected by gravity. In addition, the velocity profile of the arm is approximately bell-shaped, not perfectly bell-shaped.

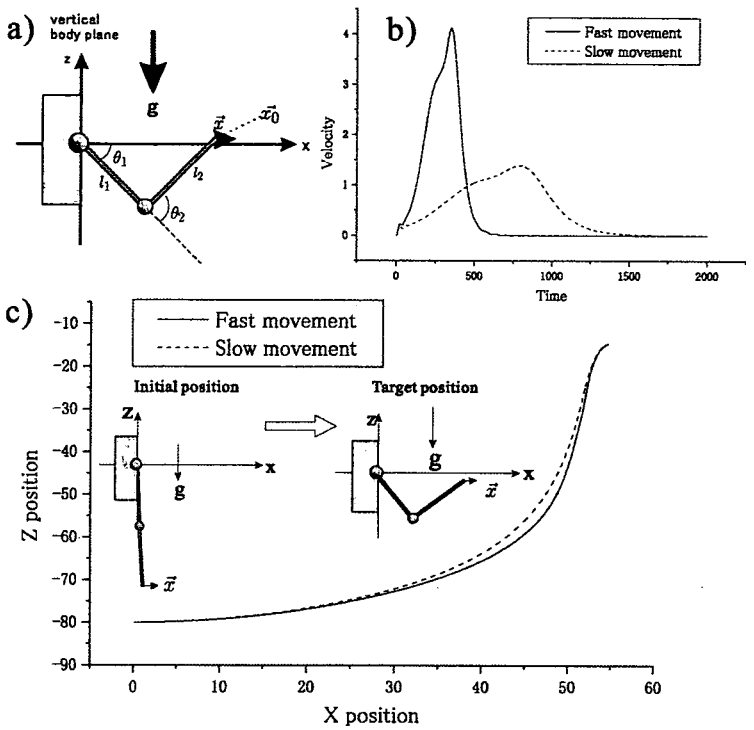

Figure 9. Two-link arm reaching movement under gravity in 2D space. (a) Diagram of the two-link model. (b) Velocity dependency of the different speed movement controls. (c) The realized trajectory patterns of the end-effector of the hand.

Concerning the dependency of the link movement speed, the trajectory transition of the end-effector (Fig. 9b) shifts slightly to the right (the front of the body) when the fast and the slow movement speeds are compared with respect to the inertia of the link movement.

5. STANDING-UP MOVEMENT OF A FOUR-LINK MODEL

In order to demonstrate the effectiveness of the proposed method for redundant manipulator control, we constructed a four-link model system (Fig. 10c) and confirmed the model using a standing-up movement from a chair. The averages of eight subjects reported in Ref. [22] were used for each of the link parameters (mass and moment) in the present experiment. The result of normal speed standing-up movement of a four-link model is shown in Fig. 10. In this simulation, the center of the gravity (COG) of the four-link model is considered as the end-effector of the arm and the movement is realized by moving the COG position. The parameters of the bell-shaped speed profile control are $\alpha = 1.0$ and $\beta = 0.01$, and the cost function parameter, J, is $\mu = 1.0$. The coordinates given for the model are the